LANGMUIR Article
Cite This: Langmuir 2017, 33, 12865-12872 pubs.acs.org/Langmuir

Graphene as Barrier to Prevent Volume Increment of Air Bubbles over Silicone Polymer in Aqueous Environment

Ruben Bartali,*[,†,‡] Andrea Lamberti,[§] Stefano Bianco,[§] Candido F. Pirri,[§] Manoj Tripathi,[∥] Gloria Gottardi,[†] Giorgio Speranza,[†] Erica Iacob,[†] Nicola Pugno,[∥,⊥,#] and Nadhira Laidani[†]

[†]Fondazione Bruno Kessler, Center for Materials and Microsystems, via Sommarive 18, 38123 Povo, Trento, Italy
[‡]Dipartimento di Fisica, Università di Trento, via Sommarive 14, 38123 Povo, Trento, Italy
[§]Applied Science and Technology Department, Politecnico di Torino, Corso Duca degli Abruzzi 24, Turin IT-10129, Italy
[∥]Laboratory of Bio-Inspired and Graphene Nanomechanics, Department of Civil, Environmental and Mechanical Engineering, University of Trento, 38123 Trento, Italy
[⊥]School of Engineering and Materials Science, Queen Mary University of London, Mile End Road, E1 4NS London, United Kingdom
[#]Ket Lab, Edoardo Amaldi Foudation, Italian Space Agency, Via del Politecnico snc, 00133 Rome, Italy

Supporting Information

ABSTRACT: The interaction of air bubbles with surfaces immersed in water is of fundamental importance in many fields of application ranging from energy to biology. However, many aspects of this topic such as the stability of surfaces in contact with bubbles remain unexplored. For this reason, in this work, we investigate the interaction of air bubbles with different kinds of dispersive surfaces immersed in water. The surfaces studied were polydimethylsiloxane (PDMS), graphite, and single layer graphene/PDMS composite. X-ray photoelectron spectroscopy (XPS) analysis allows determining the elemental surface composition, while Raman spectroscopy was used to assess the effectiveness of graphene monolayer transfer on PDMS. Atomic force microscopy (AFM) was used to study the surface modification of samples immersed in water. The surface wettability has been investigated by contact angle measurements, and the stability of the gas bubbles was determined by captive contact angle (CCA) measurements. CCA measurements show that the air bubble on graphite surface exhibits a stable behavior while, surprisingly, the volume of the air bubble on PDMS increases as a function of immersion time (bubble dynamic evolution). Indeed, the air bubble volume on the PDMS rises by increasing immersion time in water. The experimental results indicate that the dynamic evolution of air bubble in contact with PDMS is related to the rearrangement of surface polymer chains via the migration of the polar groups. On the contrary, when a graphene monolayer is present on PDMS, it acts as an absolute barrier suppressing the dynamic evolution of the bubble and preserving the optical transparency of PDMS.

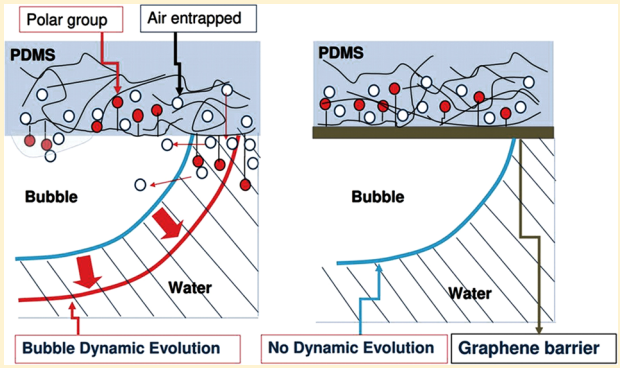

INTRODUCTION

Wettability of surfaces is widely studied in literature because the wetting characteristic of materials is crucial for many applications such as microfluidics, self-cleaning surfaces, water-repellent surfaces, bacterial adhesion, ophthalmic membranes, and microelectronics.[1−11] Moreover, liquid−solid interaction has attracted scientific interest in the field of nanoscience. For example, Rafiee and co-workers studied the water transparency of 2D materials.[12,13] Most scientific studies focused on the interaction of water drops on a surface and in air environment; only a few papers studied the complementary system composed by a bubble of gas in contact with surfaces immersed in liquid media.[14,15] However, a bubble in contact with a surface immersed in liquid could have an enormous impact in many fields, for example, on the embolism evolution investigation. Avoiding intravascular gas bubbles is vital to the health. Indeed, embolism is one of the main causes of neurocognitive dysfunction in cardiopulmonary surgery. Suzuki and Eckmann studied the adhesion force of air bubbles in the microvessesl (arterioles) of mesenteric tissue.[16] They observed that the adhesion force depends on residence time and on the presence of endothelium, thus being related to the physic-chemical structure of the internal surface. Another interesting example where the bubbles in contact with a surface can play an important role is a direct methanol fuel cell. Indeed, the behavior of the CO_2 bubbles in contact with materials immersed in liquids is a key factor to improve the performance of the device.[17] The high methanol flow rate results in small

Received: August 17, 2017
Revised: October 9, 2017
Published: October 18, 2017

DOI: 10.1021/acs.langmuir.7b02915
Langmuir 2017, 33, 12865−12872

discrete CO_2 gas bubbles and short gas slugs that increase the cell performance. However, the adhesion of the gas bubbles on the surface of materials immersed in water is not entirely understood, and an example is the unexpected nanobubbles stability on graphite immersed in water.[18,19] The thermodynamic properties, the stability, the role of surface structure/chemistry, and the role of chemical nature of the bubbles in many liquid−solid systems are still poorly understood.

The intermolecular forces in the gases are due to the nonbonding interactions as induced dipole−induced dipole interactions, known as dispersion forces.[20] In order to study an homogeneous system, herein we exploit captive bubble contact angle measurements (see the Supporting Information) to characterize the interaction of the gas bubbles with different kinds of dispersive surfaces: PDMS (polymer chains), graphite (rigid honeycomb structure), and graphene on PDMS (honeycomb structure + polymer chains). PDMS and graphite are reported in the literature as dispersive surfaces, and they are interesting from a technological point of view because they are widely used in many applications and studies.[21−24] PDMS, in particular, is used as an electrical isolator, as a structural material for microfluidic devices, or as a gas-permeable membrane.[25,26] In many applications, PDMS remains for a long time immersed in contact with water and often in contact with air bubbles. The interaction of the PDMS surface immersed in water was extensively studied in the literature.[27−31] On the contrary, studies regarding the bubble behavior in contact with PDMS surface were not reported. In this work, we studied the interaction of PDMS immersed in water in contact with air bubbles. The behavior of PDMS is compared with results obtained on graphite. Graphite shows a dispersive surface, like PDMS, but it is characterized by a lamellar crystalline lattice. In addition, graphite has a 2D parent system, namely, graphene, constituted by a single layer of sp^2-hybridized carbon atoms arranged in six-membered rings in a honeycombed network.[32−35] Due to this peculiar structure, graphene can be used as a thin blanket to protect a surface of materials from the environmental conditions.[35−39] For this reason, we covered the PDMS surface with a graphene layer, and we studied the influence of the graphene layer on gas−surface interactions. In the first part of the paper, we describe the surface chemistry, wettability, and surface tension of PDMS and graphite. In the second part of the paper, we discuss the interaction of the bubble with PDMS and graphite immersed in water. Finally, the interaction of the air bubble with a single layer graphene on PDMS surface (graphene/PDMS) is presented and the results compared with the bare PDMS material.

EXPERIMENTAL SECTION

Materials. PDMS membranes were prepared by mixing the polymer base and the curing agent (Sylgard 184, Dow Corning) in a 10:1 mixing ratio (oligomer/curing agent) and degassing in low vacuum for 1 h. The mixture was then poured into PMMA molds with an area of 2 cm^2 and depth of 1 mm (fabricated by milling machine) and cured in a convection oven following two different thermal treatments. One set of samples was cured for 1 h at 60 °C (bare PDMS sample), while another set was cured for 30 min at 60 °C. This soft curing step was performed to allow a partial cross-linking of the material, that produces a soft hardening of the membrane. As already reported by Lamberti et al.,[26] this strategy allows facilitation of the subsequent bonding of the PDMS membrane with other surfaces, permitting the later graphene transfer. The growth of single-layer graphene is performed using a cold-wall chemical vapor deposition (CVD) system. The synthesis procedure is carried out on high-quality copper foils and foresees the catalytic decomposition of carbon precursor (CH_4) in a high-temperature deposition process (1000 °C) in the reactive H_2/Ar atmosphere (Ar/H_2/CH_4 partial pressure: 80:10:10). The growth process can guarantee the controlled formation of single-layer graphene with reduced defectiveness. The graphene/Cu substrate is transferred on the partially reticulated PDMS surface, obtaining an excellent adhesion between the elastomeric substrate and the G/Cu film during the final reticulation procedure performed for other 30 min at 60 °C. Cu layer is then removed in acidic $FeCl_3$ solution in water (2.25 M for 1 h).

Graphite samples were prepared by mechanical exfoliation of highly oriented pyrolytic graphite (HOPG) (Goodfellow Cambridge). The thickness of exfoliated graphite was 14 μm; the lateral size was 10 mm × 10 mm, and the resistivity was 8×10^{-5} Ω·cm. The contact angle on the PDMS and graphene/PDMS surface was measured on the sample as received (aged surfaces).

Methods. The surface free energy was calculated by contact angle measurements following the Owens−Wendt approach.[54] The total surface energy γ_s in the Owens−Wendt approach is defined as the sum of polar and dispersive components indicated as γ_s^p and γ_s^d, respectively:

$$\gamma_s = \gamma_s^p + \gamma_s^d \quad (1)$$

where the dispersive component is due to London interactions and polar components are the sum of hydrogen, polar, inductive and acid−base interactions. By the Owens−Wendt method, the surface energy can be estimated by the following equation:

$$(1 + \cos\theta)\gamma_l = 2\sqrt{\gamma_s^d \gamma_l^d} + 2\sqrt{\gamma_s^p \gamma_l^p} \quad (2)$$

where θ is the contact angle, γ_l the total surface tension of liquids, γ_l^d is the dispersive component of the fluids, and γ_l^p is a polar component of the fluids. Due to two unknown parameters (γ_s^p and γ_s^d) in eq 1, the contact angle has to be measured using two liquids with known properties, one dispersive liquid and one polar liquid. In this study, static contact angle measurements for surface energy estimation were performed with Milli-Q deionized water and diiodomethane. These two liquids have been used since diiodomethane has only a dispersive component and water has a dominant polar component. The total surface energy of liquids and their polar and nonpolar components are listed in Table 1.

Table 1. Surface Energy Components of the Probe Liquids (mJ/m^2)[a55]

liquids	γ_l	γ_l^d	γ_l^p
water	72.8	21.8	51
diiodomethane	52.8	52.8	≈0

[a]Total surface tension γ_l, the dispersive components γ_l^d and the polar components γ_l^p of the liquids in mJ/m^2.

The bubble contact angle was measured using a cell of a plastic cuvette (1.5 × 1.5 cm^2) filled with deionized water, (see Supporting Information S1). The examined materials were immersed in the liquid and air bubbles were placed under the surface of the tested materials using a calibrated syringe. The evaluation of the bubble volume has been done using Drop Analysis software.[56]

The atomic force microscope has been used to operate live imaging in deionized water as well as in air conditions using a silicon probe (model: CSG01), with nominal radii < 10 nm. The imaging and measurements were carried out in contact mode in liquid environment for the samples immersed in water for 24 and 48 h at room temperature (25−30 °C). Raman analysis was performed using a Renishaw InVia Reflex micro-Raman spectrometer (Renishaw plc, Wottonunder-Edge, UK), equipped with a cooled CCD camera. A laser diode source (λ_{ex} = 514.5 nm, power ∼ 5 mW) was used, and sample inspection occurred through a microscope objective (50×), with backscattering light collection.

DOI: 10.1021/acs.langmuir.7b02915
Langmuir 2017, 33, 12865−12872

Table 2. Chemical Surface Composition and Surface Energy of Graphite, PDMS, and Graphene-PDMS

	XPS, atom %			surface energy (Owens–Wendt), mJ/m^2		
	carbon	oxygen	silicon	total	dispersive	polar
PDMS	53.5 ± 0.5	26.86 ± 0.3	19.6 ± 0.2	25.8 (±2.5)	25.7 (±2.4)	0.1 (±0.1)
graphite	98.5 ± 0.9	1.5 ± 0.1		52.2 (±3)	50.8 (±2.8)	2.2 (±0.2)
PDMS + graphene	54.2 ± 0.4	26.3 ± 0.2	19.4 ± 0.2	33 (±2)	32.9 (±1.9)	0.1 (±0.1)

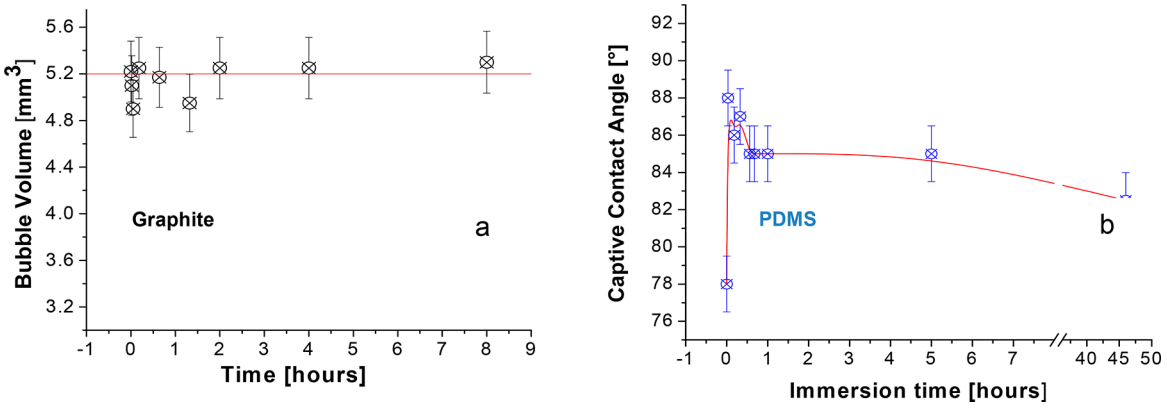

Figure 1. Air bubble volume on (a) graphite and (b) captive contact angle on PDMS as a function of the time.

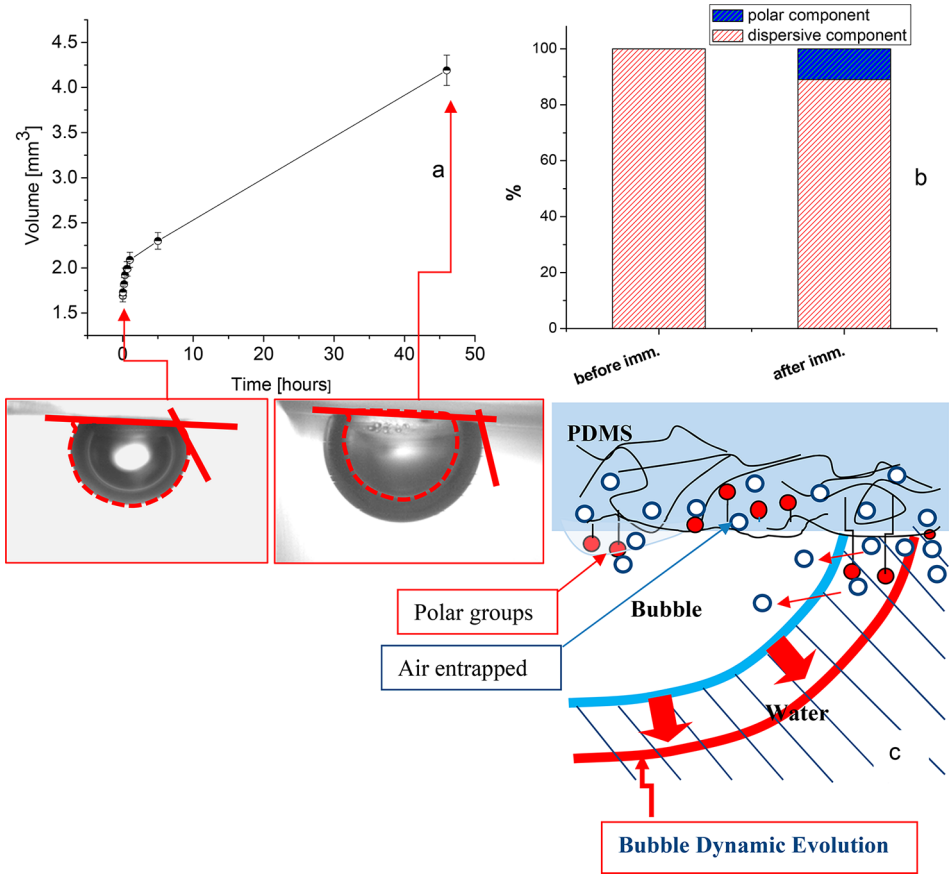

Figure 2. Variation of bubble contact angle after immersion in water (a) and variation of the polar and dispersive components before and after soaking procedure (b) on PDMS and sketch of bubble dynamic evolution on PDMS (c).

RESULT AND DISCUSSION

The surface chemistry of exfoliated graphite (EG) and polydimethylsiloxane (PDMS) provided by XPS analysis is summarized in Table 2. The survey spectra of XPS on EG show, as expected, the presence of carbon and a small amount of oxygen, due to contamination. The surface chemistry of the PDMS indicates the presence of carbon, oxygen, and silicon. The percentage of carbon and oxygen on PDMS is less than the theoretical value (50 and 25%, respectively), while the proportion of silicon is slightly higher of theoretical one (i.e.,

DOI: 10.1021/acs.langmuir.7b02915
Langmuir 2017, 33, 12865−12872

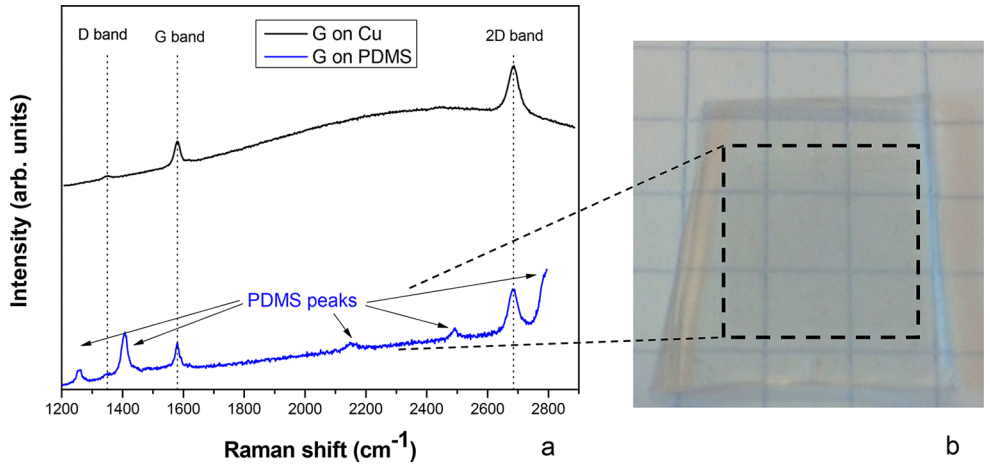

Figure 3. Raman spectra of graphene on Cu (black line) and PDMS (blue line) (a). Image of graphene/PDMS (b); the graphene/PDMS sample remains transparent.

15%). The unbalanced surface stoichiometry is typical of slightly aged PDMS as reported in the literature.[40]

Through drop shape angle measurement, we found an average water contact angle of 80° ± 2° on graphite, typical of slightly aged graphite,[41] and 107° ± 2° on PDMS. (The authors underline that some samples of PDMS show a CA of 105° ± 2°.) The diiodomethane, which is a dispersive liquid, showed contact angles lower than 10° on graphite and higher than 60° on PDMS. The total surface energy of graphite was 52.2 mJ/m^2, and more of the 95% of surface energy was due to dispersive components. Only a small component of the surface (4.4%) derived from the polar component; the polar component was probably due to the contaminations, as corroborated by XPS findings. The PDMS shows a surface energy value lower than that of graphite, as indicated by the contact angle of diiodomethane, i.e., 25.5 mJ/m^2. The interaction of the air bubble with the surface has been studied using the captive bubble contact angle. Subsequently, exfoliated graphite was then immersed in water and the interaction of air bubbles with the surface has been studied using CCA. The air captive contact angle on graphite was around 82° and as already reported by the authors it remains stable as a function of immersion time.[42] The bubble contact angle stability appears in contrast to the trend reported in the literature with sessile contact angles,[41,43−45] since the immersion procedure tends to keep the surface cleaner thus reducing airborne contamination to that deriving from the small volume of the bubble. In the same way, we also estimated the volume of the bubble, using Drop Analysis software.[53]

Figure 1a shows the time evolution of volume of the bubble in contact with graphite surface; the air bubble volume on graphite remains within the experimental error constant. The bubble test has been performed on PDMS surface. We observed an increase of the captive contact angle from 78° to 88°, an instability of contact angle in the first 20 min, after an increase, and finally a stabilization of the CCA at 83−84°; see Figure 1b. The initial increase of CCA is probably due to presence of surface contaminations. The reduction in CCA, after initial stage, was expected since Hillborg et al.[27,46] and Gustavsson et al.[28] reported the variation of sessile contact angle after the immersion of PDMS in water. They reported that reduction of hydrophobicity on PDMS is due to the migration of the polar group at the surface of the polymer when the polymers are immersed in water. Moreover, the permeation of water induces also the formation of polar Si−OH groups due to hydrolysis of the PDMS backbone.[47] In this experiment, surprisingly, we also observed an increase in the bubble volume (see Figure 2a). The starting volume was 1.69 mm^3, while after 5 h the volume became 2.03 mm^3, i.e., an increase of 21%. To corroborate this result, the immersion time was extended up to 46 h. After 46 h, we measured a contact angle of 82.5° and a volume of 4.03 mm^3; that means an increase of 238%. The inset of Figure 2a shows the images of the bubble at the beginning of the test and after 46 h. The red line in the picture reported in Figure 2a indicates the original bubble profile. The variation of the bubble volume means that there is a source of gas. The source of gas can be endogenous as gas in water or PDMS or exogenous as the air flow from outside of captive bubble cell. Therefore, in a first approximation, (a) the source can be due to the coalescence of microbubbles/nanobubbles dissolved in water, (b) it is related to surface phenomena of PDMS, and/or (c) it is related to the permeation of the gas from the external side of PDMS exposed to the atmosphere to the side exposed to the water. Considering the experimental conditions, we could exclude the permeation of the gas due to a differential pressure between the external pressure and bubble pressure since inside the bubble there is a small positive overpressure. The overpressure inside the bubble was estimated by Young−Laplace equation and was around 40 mbar.[48] We cannot ignore the fact that the increase of bubble volume can be due to the coalescence of microbubbles but the stability of bubble volume on graphite indicates that the coalescence of micronanobubbles in a first approximation is negligible. The variation of PDMS captive contact angle, reported in Figure 1b, indicates a change in surface chemistry.

To better understand the surface modification during the immersion, we estimated the polar components present on the surface of PDMS before and after the immersion/soaking procedure using Owens − Wendt method. The results show that, before immersion, the surface of PDMS was totally dispersive and after 5 h of immersion 10% of the surface shows a polar behavior, indicating, as reported by Kennan et al.[49] and Hillbolrg et al.,[27,46] a migration of polar groups on the surface when the PDMS is contact with water (Figure 2b). The migration of polar groups in polymer chains can promote the rotation and the movement of the chains of PDMS. PDMS has a porous structure, and the air is entrapped in these pores. Therefore, the rearrangement and movement of polymer chains

DOI: 10.1021/acs.langmuir.7b02915
Langmuir 2017, 33, 12865−12872

promotes the transport of the air from the polymer structure to the PDMS external surface; this process is accomplished by the percolation of water inside the first layers of PDMS due to diffusion process.[27] Ismail et al.,[50] in fact, revealed that a centralized oxygen molecule from water could diffuse through methyl terminated PDMS which causes the "caging" and "hopping" phenomenon. The diffusion of water in the first layers of PDMS, that is a source of degradation of the PDMS backbone, can help in the removal of air from polymer pores.[28] The air molecules that are coming from the PDMS structure, due to the geometrical constraint of the CCA system (surface in contact with bubble and water under the PDMS sample), are obligated to move on the surface of the polymer until they nucleate in a bubble (see Figure 2c). As a result of the rearrangement, the surface structure of PDMS in water acts as a small source of the flux of gas that can inflate the bubble. We noted that, in the interior region of the bubble, due to the high relative humidity, there are condensed drops (see the Supporting Information). The formation of a thin layer of condensed water can promote, as in immersion in water, the migration of polar groups on the polymer chains. To verify the hypothesis that the inflating mechanism is due to surface modification induced by water, we deposit a 2D layer of graphite, i.e., single-layer graphene, as a barrier on PDMS. The graphene layer was employed to (a) have a rigid surface to avoid the dynamic rearrangement of the surface and (b) to inhibit the interaction of water and polar groups and diffusion of water. In Figure 3, Raman spectra and the drop shape contact angle on PDMS coated with graphene are reported. As-deposited graphene on copper foil shows the presence of the G band at ~1580 cm^{-1} (due to the first order inelastic scattering process involving the degenerate iTO and iLO phonons at the G point, E_{2g} mode) and of the 2D band at ~2700 cm^{-1} (related with the second-order zone-boundary phonons). The D peak at ~1350 cm^{-1}, related with the defectiveness of the hexagonal carbon lattice, is not revealed in the spectrum. The described features are superimposed to a luminescent behavior, related to the metallic supporting substrate. The intensity ratio between the G and 2D peaks mirrors the high quality of the graphene film. The transfer of graphene on PDMS does not dramatically affect the quality of the graphene layer. By contact angle, we observed a sensible reduction of water contact angle on graphene/PDMS, from 107° to less than 100°, a wetting more similar to that of graphite surface. The increase of the surface energy, as indicated in Table 2, and the presence of the G and 2D peaks in the Raman spectra confirm that graphene layers cover the surface. It is interesting to observe in the image photograph (inset Figure 3b) that the graphene/PDMS sample preserved its optical transparency, in agreement with low optical absorption of a single layer of graphene.

Figure 4a shows the bubble volume normalized to the initial volume of the bubble, on the PDMS surface and on graphene/PDMS. The comparison clearly shows that in the system composed by graphene/PDMS the bubble size remains unchanged. The captive contact angle of graphene/PDMS surface is reported in Figure 4b. We observed an initial increase of captive contact angle on the surface from 78° to 87°. Similarly to the case of PDMS, we could expect that the variation in the early stage of the experiment is due to contamination.[42,43] After the initial stage, the CCA remains unchanged because the water cannot physically pass through the graphene barrier layer to continuously promote the

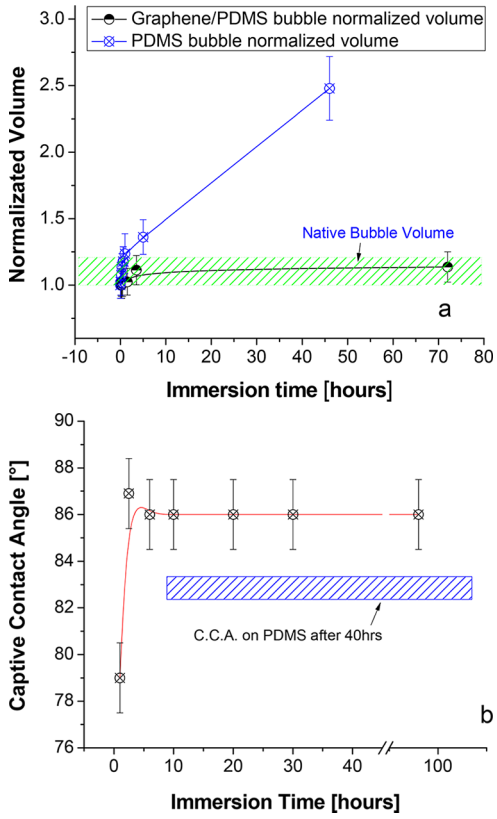

Figure 4. Bubble behavior on the graphene/PDMS surface, with the relative volume of the bubble as a function of immersion time (a) and CCA on graphene/PDMS (b).

migration of the polar group, this is corroborated by the stabilization of the bubble contact angle at 86°.

To understand better the morphological changes of surfaces at the nanoscale in water, we characterized the materials using AFM equipped with a head for measurements in liquid. The interface of DI water over PDMS was analyzed through AFM in contact mode operation, and live imaging was carried out in water. Figure 5 shows the AFM image of PDMS (a–c) and Gr/PDMS (d–f) in the air and water. In the air condition, roughness (rms) of PDMS and Gr/PDMS was measured as 2.6 ± 0.33 nm and 7.9 ± 0.8 nm, respectively. Higher roughness of the graphene covered PDMS is achieved by the presence of graphene wrinkles; see Figure 5a and d. The topography of PDMS gradually changes in water medium with the progression of time. Roughness has been increased up to 5 times at different time intervals up to 48 h after the immersion (see the Supporting Information). The AFM results in combination with the result of surface polarity (Figure 2b) confirm that on PDMS there is a rearrangement of polymer chains due to the migration of polar groups that induce, with inevitable diffusion of water, a sensible modification of morphology. Nevertheless, the topology of the graphene covered PDMS remains unaffected in similar conditions. Figure 5 shows the ability of graphene to protect the PDMS substrate from water molecules. A similar phenomenon has been observed by Wang et al.[51] to protect the silica glass surface from corrosion in water through implementation of CVD graphene as a barrier. In Figure 6, we report for PDMS and graphene/PDMS the variation of the volume of the bubble versus the change of roughness acquired by AFM in liquid (both parameters have been normalized to 1). We can observe that there is a direct correlation between the

DOI: 10.1021/acs.langmuir.7b02915
Langmuir 2017, 33, 12865–12872

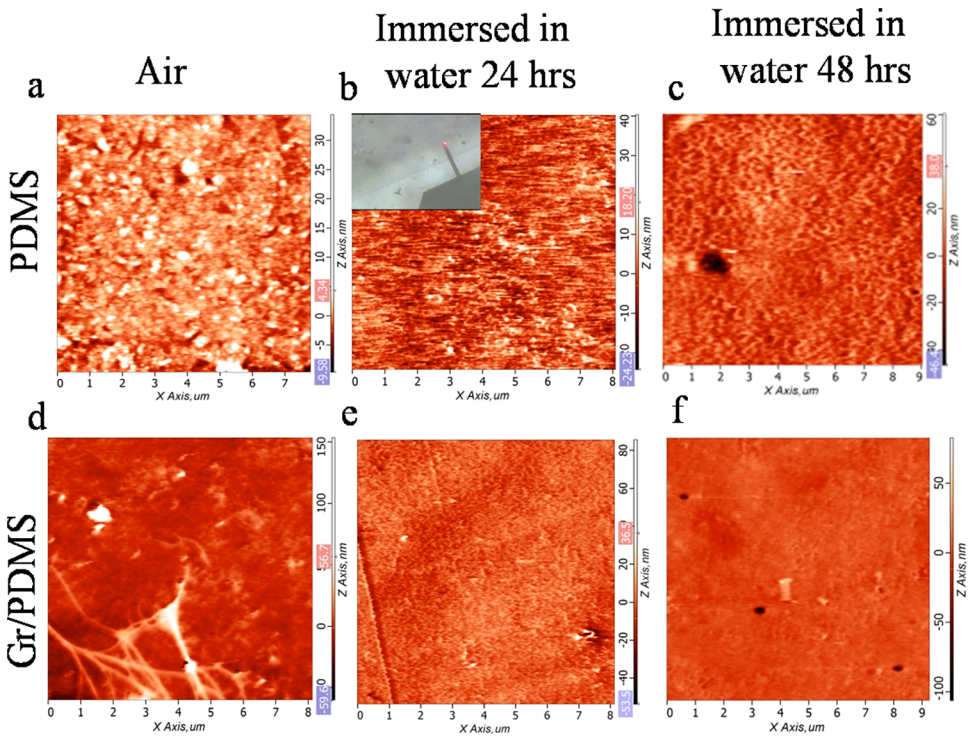

Figure 5. AFM topography of PDMS and graphene covered PDMS (Gr/PDMS) in air and water conditions after 24 and 48 h. Inset in panel (b) shows the live imaging of the sample immersed in water.

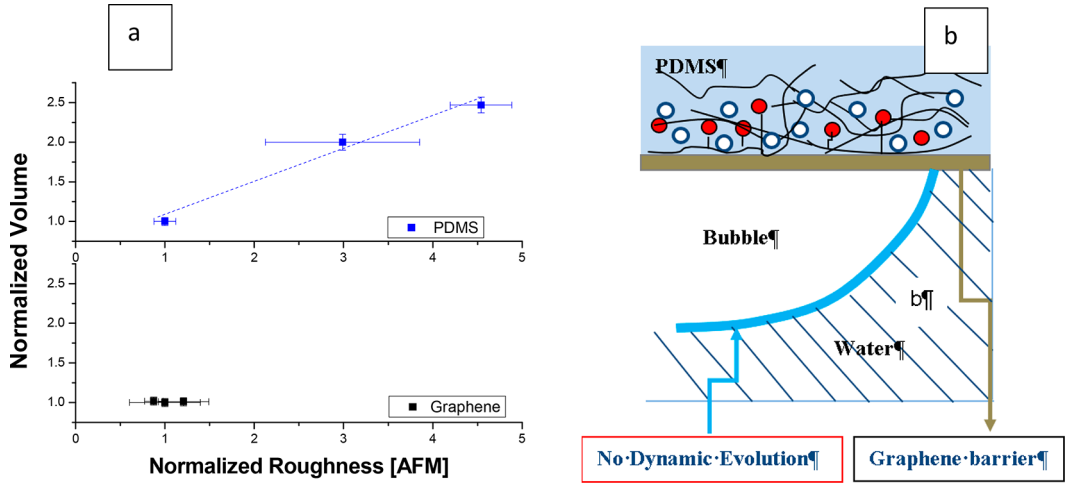

Figure 6. Variation of bubble volumes against variation of roughness during immersion in water; roughness has been estimated using AFM in liquid (a). Barrier effect of graphene (b).

increase of the roughness and the dynamic evolution of bubble volume; see blue dots of PDMS the surface in Figure 6. On graphene/PDMS, no significant variation of roughness has been observed and no sensible change of bubble volume has been recognized

The direct relationship between roughness evolution in water and the trend of bubble volume confirms that the dynamic evolution on PDMS is related to rearrangement of surface polymer chains as well as the diffusion of water in the polymer structure. The graphene layer inhibits almost entirely the interaction of water with PDMS surface and inhibits almost entirely the inflating of the air bubble increasing the PDMS surface stability, Figure 6b. This behavior is also in line with previous reported studies on the permeation properties of single layer graphene as an absolute gas barrier.[52]

We remark that even if the positive protective effect of graphene on PDMS surface was demonstrated, the full comprehension of captive contact angle and the inflating mechanism of the bubble in contact with the polymer is not reached. We did not consider, for instance, the effect of the evolution of nano/microcorrugation on the captive bubble that could play an important role in the assessment of CCA. At the nanoscale, in fact, the modification of the morphology of the surface can change the wetting mode, e.g., the Wenzel mode, Penetrate mode, or Cassie−Baxter mode, and therefore can induce different CCA. The authors underline that further investigations, in particular using computational modeling, are

DOI: 10.1021/acs.langmuir.7b02915
Langmuir 2017, 33, 12865−12872

necessary to obtain a robust assessment of the effect of nano/microcorrugation on captive contact angle.[53] This is corroborated by the fact that captive contact angle is in many cases the value measured on the same material by sessile contact angle measurement; probably the spread of liquid (penetrate model) and the spread of gas near the triple point have to be taken into consideration to obtain a more accurate description of the captive contact angle. Further work is necessary to understand the dynamic behavior of the bubbles better, but we think that this topic could open new opportunities to reduce the risk of embolism in bioimplants. Moreover, we believe that the management of dynamic evolution of the bubble by means of 2D materials could open a new opportunity for nano/microfluidics such as selective permeation of gas and gas storage at the nanoscale.

CONCLUSION

In this work, we studied the interaction of air bubbles with different types of dispersive surfaces. We observed that a bubble on graphite surface shows a stable behavior. While, we observed that the bubble in contact with PDMS shows a dynamic evolution as a function of time of immersion. The results obtained on captive contact angle, the morphological evolution of polymer recognized by AFM in liquid ,and the variation of thermodynamical properties obtained by Owens−Wendt method indicated that this response is related to the rearrangement of the polymer structure on the surface due to the migration of polar groups on the surface. The polymer chain rearrangement on the surface of PDMS and water diffusion, that transfer the air from the bulk of polymer to the surface, behave as a supplementary source of gas that inflate the bubble in contact with the material. The experiments show that this effect can be entirely avoided using a graphene layer as a barrier without losing the optical transparency in the visible PDMS material. We remark that more work is necessary to understand better the progressive increase of the bubble volume. However, we believe that the effect can open new opportunities in nanofluidic fields in which air bubbles play a significant role.

ASSOCIATED CONTENT

Supporting Information

The Supporting Information is available free of charge on the ACS Publications website at DOI: 10.1021/acs.langmuir.7b02915.

Further information about sessile contact angle and captive contact angle setup; roughness of samples immersed in water (PDF)

AUTHOR INFORMATION

Corresponding Author

*E-mail: bartali@fbk.eu

ORCID

Ruben Bartali: 0000-0003-2275-9037

Nicola Pugno: 0000-0003-2136-2396

Notes

The authors declare no competing financial interest.

ACKNOWLEDGMENTS

N.P. is supported by the European Research Council PoC 2015 "Silkene" No. 693670, by the European Commission H2020 under the Graphene Flagship Core 1 No. 696656 (WP14 "Polymer composites"), and under the Fet Proactive "Neurofibers" No. 732344.

REFERENCES

(1) Berdichevsky, Y.; Khandurina, J.; Guttman, A.; Lo, Y. H. UV/ozone Modification of Poly(dimethylsiloxane) Microfluidic Channels. *Sens. Actuators, B* **2004**, *97*, 402−408.

(2) Zhang, M.; Feng, S.; Wang, L.; Zheng, Y. Lotus Effect in Wetting and Self-Cleaning. *Biotribology.* **2016**, *5*, 31−43.

(3) Gezer, P. G.; Brodsky, S.; Hsiao, A.; Liu, G. L.; Kokini, J. L. Modification of the Hydrophilic/Hydrophobic Characteristic of Zein film Surfaces by Contact with Oxygen Plasma Treated PDMS and Oleic Acid Content. *Colloids Surf., B* **2015**, *135*, 433−440.

(4) Onda, T.; Shibuichi, S.; Satoh, N.; Tsujii, K. Super-Water-Repellent Fractal Surfaces. *Langmuir* **1996**, *12*, 2125−2127.

(5) Zhao, Q.; Wang, C.; Liu, Y.; Wang, S. Bacterial Adhesion on the Metal-Polymer Composite Coatings. *Int. J. Adhes. Adhes.* **2007**, *27*, 85−91.

(6) Bodas, D.; Khan-Malek, C. Formation of More Stable Hydrophilic Surfaces of PDMS by Plasma and Chemical Treatments. *Microelectron. Eng.* **2006**, *83*, 1277−1279.

(7) Vassallo, E.; Cremona, A.; Ghezzi, F.; Ricci, D. Characterization by Optical Emission Spectroscopy of an Oxygen Plasma Used for Improving PET Wettability. *Vacuum* **2010**, *84*, 902−906.

(8) Francioso, L.; De Pascali, C.; Bartali, R.; Morganti, E.; Lorenzelli, L.; Siciliano, P.; Laidani, N. PDMS/kapton Interface Plasma Treatment Effects on the Polymeric Package for a Wearable Thermoelectric Generator. *ACS Appl. Mater. Interfaces* **2013**, *5*, 6586−6590.

(9) Clair, S.; Variola, F.; Kondratenko, M.; Jedrzejowski, P.; Nanci, A.; Rosei, F.; Perepichka, D. F. Self-Assembled Monolayer of Alkanephosphoric Acid on Nanotextured Ti. *J. Chem. Phys.* **2008**, *128*, 144705.

(10) Petersson, L.; Meier, P.; Kornmann, X.; Hillborg, H. Effect of Surface Cleanliness of Aluminium Substrates on Silicone Rubber Adhesion. *J. Phys. D: Appl. Phys.* **2011**, *44*, 034011.

(11) Juárez-moreno, J. A.; Ávila-ortega, A.; Oliva, A. I.; Avilés, F.; Cauich-rodríguez, J. V. Applied Surface Science Effect of Wettability and Surface Roughness on the Adhesion Properties of Collagen on PDMS Films Treated by Capacitively Coupled Oxygen Plasma. *Appl. Surf. Sci.* **2015**, *349*, 763−773.

(12) Rafiee, J.; Rafiee, M. A.; Yu, Z.-Z.; Koratkar, N. Superhydrophobic to Superhydrophilic Wetting Control in Graphene films. *Adv. Mater.* **2010**, *22*, 2151−2154.

(13) Rafiee, J.; Mi, X.; Gullapalli, H.; Thomas, A. V.; Yavari, F.; Shi, Y.; Ajayan, P. M.; Koratkar, N. A. Wetting Transparency of Graphene. *Nat. Mater.* **2012**, *11*, 217−222.

(14) Drelich, J.; Miller, J. D.; GooD, R. The Effect of Drop (Bubble) Size on Advancing and Receding Contact Angles for Heterogeneous and Rough Solid Surfaces as Observed with Sessile-Drop and Captive-Bubble Techniques. *J. Colloid Interface Sci.* **1996**, *179*, 37−50.

(15) Maiolo, D.; Federici, S.; Ravelli, L.; Depero, L. E.; Hamad-Schifferli, K.; Bergese, P. Nanomechanics of Surface DNA Switches Probed by Captive Contact Angle. *J. Colloid Interface Sci.* **2013**, *402*, 334−339.

(16) Suzuki, A.; Eckmann, D. M. Embolism Bubble Adhesion Force in Excised Perfused. *Anesthesiology* **2003**, *99*, 400−408.

(17) Liao, Q.; Zhu, X.; Zheng, X.; Ding, Y. Visualization Study on the Dynamics of CO2 bubbles in Anode Channels and Performance of a DMFC. *J. Power Sources* **2007**, *171*, 644−651.

(18) Lu, Y.-H.; Yang, C.-W.; Fang, C.-K.; Ko, H.-C.; Hwang, I.-S. Interface-Induced Ordering of Gas Molecules Confined in a Small Space. *Sci. Rep.* **2015**, *4*, 7189.

(19) Sun, Y.; Xie, G.; Peng, Y.; Xia, W.; Sha, J. Stability Theories of Nanobubbles at Solid−Liquid Interface: A review. *Colloids Surf., A* **2016**, *495*, 176−186.

(20) Hohm, U. Experimental Static Dipole−Dipole Polarizabilities of Molecules. *J. Mol. Struct.* **2013**, *1054-1055*, 282−292.
(21) Sun, M.; Luo, C.; Xu, L.; Ji, H.; Ouyang, Q.; Yu, D.; Chen, Y. Artificial Lotus Leaf by Nanocasting. *Langmuir* **2005**, *21*, 8978−8981.
(22) Stanton, M. M.; Ducker, R. E.; MacDonald, J. C.; Lambert, C. R.; McGimpsey, W. G. Super-Hydrophobic, Highly Adhesive, Polydimethylsiloxane (PDMS) surfaces. *J. Colloid Interface Sci.* **2012**, *367*, 502−508.
(23) Preston, D. J.; Mafra, D. L.; Miljkovic, N.; Kong, J.; Wang, E. N. Scalable Graphene Coatings for Enhanced Condensation Heat Transfer. *Nano Lett.* **2015**, *15*, 2902−2909.
(24) Kozbial, A.; Trouba, C.; Liu, H.; Li, L. Characterization of the Intrinsic Water Wettability of Graphite Using Contact Angle Measurements : Effect of Defects on Static and Dynamic Contact Angles. *Langmuir* **2017**, *33*, 959−967.
(25) Lamberti, A.; Quaglio, M.; Sacco, a.; Cocuzza, M.; Pirri, C. F. Surface Energy Tailoring of Glass by Contact Printed PDMS. *Appl. Surf. Sci.* **2012**, *258*, 9427−9431.
(26) Lamberti, A.; Marasso, S. L.; Cocuzza, M. PDMS Membranes with Tunable Gas Permeability For Microfluidic Applications. *RSC Adv.* **2014**, *4*, 61415−61419.
(27) Hillborg, H.; Gedde, U. W. Hydrophobicity Changes in Silicon Rubbers. *IEEE Trans. Dielectr. Electr. Insul.* **1999**, *6*, 703.
(28) Gustavsson, T. G.; Gubanski, S. M.; Lambrecht, J. Hydratization of the PDMS Backbone During Water Immersion Test. *IEEE-CEIDP* **1998**, 269−272.
(29) Bhattacharya, S.; Datta, A.; Berg, J. M.; Gangopadhyay, S. Studies on Surface Wettability of Poly(dimethyl)siloxane (PDMS) and Glass Under Oxygen-Plasma Treatment and Correlation with Bond Strength. *J. Microelectromech. Syst.* **2005**, *14*, 590−597.
(30) Bodas, D.; Khan-Malek, C. Hydrophilization and Hydrophobic Recovery of PDMS by Oxygen Plasma and Chemical Treatment-An SEM Investigation. *Sens. Actuators, B* **2007**, *123*, 368−373.
(31) Hillborg, H.; Tomczak, N.; Olah, A.; Schonherr, H.; Vancso, G. J. Nanoscale Hydrophobic Recovery : A Chemical Force Microscopy Study of UV/Ozone-Treated Cross-Linked Poly (dimethylsiloxane). *Langmuir* **2004**, *20*, 785−794.
(32) Geim, A. K.; Novoselov, K. S. The Rise of Graphene. *Nat. Mater.* **2007**, *6*, 183−191.
(33) Stankovich, S.; Dikin, D. A.; Piner, R. D.; Kohlhaas, K. A.; Kleinhammes, A.; Jia, Y.; Wu, Y.; Nguyen, S. T.; Ruoff, R. Synthesis of Graphene-Based Nanosheets Via Chemical Reduction of Exfoliated Graphite Oxide. *Carbon* **2007**, *45*, 1558−1565.
(34) Ebrahimi, M.; Rosei, F. Organic Analogues of Graphene. *Nature* **2017**, *542*, 423.
(35) Petucci, J.; LeBlond, C.; Karimi, M.; Vidali, G. Diffusion, Adsorption, and Desorption of Molecular Hydrogen on Graphene and in Graphite. *J. Chem. Phys.* **2013**, *139* (4), 044706.
(36) Mayavan, S.; Siva, T.; Sathiyanarayanan, S. Graphene Ink as a Corrosion Inhibiting Blanket for Iron in Aggressive Chloride Environment. *RSC Adv.* **2013**, *3*, 24868−24871.
(37) Su, Y.; Kravets, V. G.; Wong, S. L.; Waters, J.; Geim, a K.; Nair, R. R. Impermeable Barrier Films and Protective Coatings Based on Reduced Graphene Oxide. *Nat. Commun.* **2014**, *5*, 4843.
(38) Schriver, M.; Regan, W.; Gannett, W. J.; Zaniewski, A. M.; Crommie, M. F.; Zettl, A. Graphene as a Long-Term Metal Oxidation Barrier: Worse Than Nothing. *ACS Nano* **2013**, *7*, 5763−5768.
(39) Wang, B.; Cunning, B. V.; Park, S.-Y.; Huang, M.; Kim, J.-Y.; Ruoff, R. S. Graphene Coatings as Barrier Layers to. *ACS Nano* **2016**, *10*, 9794−9800.
(40) Ghanbari-Siahkali, A.; Mitra, S.; Kingshott, P.; Almdal, K.; Bloch, C.; Rehmeier, H. K. Investigation of the hydrothermal stability of cross-linked liquid silicone rubber (LSR). *Polym. Degrad. Stab.* **2005**, *90*, 471−480.
(41) Kozbial, A.; Li, Z.; Sun, J.; Gong, X.; Zhou, F.; Wang, Y.; Xu, H.; Liu, H.; Li, L. Understanding the Intrinsic Water Wettability of Graphite. *Carbon* **2014**, *74*, 218−225.
(42) Bartali, R.; Otyepka, M.; Pykal, M.; Lazar, P.; Micheli, V.; Gottardi, G.; Laidani, N. Interaction of the Helium, Hydrogen, Air, Argon, and Nitrogen Bubbles with Graphite Surface in Water. *ACS Appl. Mater. Interfaces* **2017**, *9*, 17517−17525.
(43) Li, Z.; Wang, Y.; Kozbial, A.; Shenoy, G.; Zhou, F.; McGinley, R.; Ireland, P.; Morganstein, B.; Kunkel, A.; Surwade, S. P.; Li, l.; Liu, H. Effect of Airborne Contaminants on the Wettability of Supported Graphene and Graphite. *Nat. Mater.* **2013**, *12*, 925−931.
(44) Ashraf, A.; Wu, Y.; Wang, M. C.; Aluru, N. R.; Dastgheib, S a.; Nam, S. Spectroscopic Investigation of the Wettability of Multilayer Graphene Using Highly Ordered Pyrolytic Graphite as a Model Material. *Langmuir* **2014**, *30*, 12827−12836.
(45) Wei, Y.; Jia, C. Q. Intrinsic Wettability of Graphitic Carbon. *Carbon* **2015**, *87*, 10−17.
(46) Hillborg, H.; Ankner, J. F.; Gedde, U. W.; Smith, G. D.; Yasuda, H. K.; Wikstrom, K. Crosslinked Polydimethylsiloxane Exposed to Oxygen Plasma Studied by Neutron Reflectometry and Other Surface Specific Techniques. *Polymer* **2000**, *41*, 6851−6863.
(47) Thomas, D. K. Scission Processes in Peroxide Cured Methylvnyl Silicone Rubber. *Polymer* **1966**, *7*, 99−105.
(48) Nagayama, G.; Tsuruta, T.; Cheng, P. Molecular Dynamics Simulation on Bubble Formation in a Nanochannel. *Int. J. Heat Mass Transfer* **2006**, *49*, 4437−4443.
(49) Kennan, J. J.; Peters, Y. A.; Swarthout, D. E.; Owen, M. J.; Namkanisorn, A.; Chaudhury, M. K. Effect of Saline Exposure on the Surface and Bulk Properties of Medical Grade Silicone Elastomers. 1996. *J. Biomed. Mater. Res.* **1997**, *36*, 487−497.
(50) Ismail, A. E.; Grest, G. S.; Heine, D. R.; Stevens, M. J.; Tsige, M. Interfacial Structure and Dynamics of Siloxane Systems . *Macromolecules* **2009**, *42*, 3186−3194.
(51) Wang, B.; Cunning, B. V.; Park, S.-Y.; Huang, M.; Kim, J.-Y.; Ruoff, R. S. Graphene Coatings as Barrier Layers to Prevent the Water-Induced Corrosin of Silicate Glass. *ACS Nano* **2016**, *10*, 9794−9800.
(52) Koenig, S. P.; Wang, L.; Pellegrino, J.; Bunch, J. S. Selective Molecular Sieving Through Porous Graphene. *Nat. Nanotechnol.* **2012**, *7*, 728−732.
(53) Kim, D.; Pugno, N. M.; Ryu, S. Wetting Theory For Small Droplets on Textured Solid Surfaces. *Sci. Rep.* **2016**, *6*, 37813.
(54) Rudawska, A.; Jacniacka, E. Analysis for Determining Surface Free Energy Uncertainty By the Owen−Wendt Method. *Int. J. Adhes. Adhes.* **2009**, *29*, 451−457.
(55) Gindl, M.; Sinn, G.; Gindl, W.; Reiterer, A.; Tschegg, S. A Comparison of Different Methods to Calculate the Surface Free energy of Wood Using Contact Angle Measurements. *Colloids Surf., A* **2001**, *181*, 279−287.
(56) Stalder, A. F.; Kulik, G.; Sage, D.; Barbieri, L.; Hoffmann, P. A Snake-based Approach to Accurate Determination of both Contact Points and Contact Angles. *Colloids Surf., A* **2006**, *286*, 92−103.

DOI: 10.1021/acs.langmuir.7b02915
Langmuir 2017, 33, 12865−12872

Supplementary Information

Graphene as Barrier to Prevent Volume Increment of Air Bubbles Over Silicone Polymer in Aqueous Environment..

Ruben Bartali. [*,†,‡], Andrea Lamberti [§], Stefano Bianco [§], Candido F. Pirri [§], Manoj Tripathi [‖], Gloria Gottardi [†], Giorgio Speranza [†], Erica Iacob [†]., Nicola Pugno [‖,⊥,∞], and Nadhira Laidani [†]

[†]*Fondazione Bruno Kessler,Center for Materials and Microsystems, via Sommarive 18, 38123 Povo, Trento, Italy*

[‡]*Dipartimento di Fisica , Università di Trento, via Sommarive 14, 38123 Povo, Trento , Italy*

[§] *Applied Science and Technology Department, Politecnico di Torino, Corso Duca degli Abruzzi 24, Turin, IT-10129, Italy*

[‖]*Laboratory of Bio-Inspired and Graphene Nanomechanics, Department of Civil, Environmental and Mechanical Engineering, University of Trento, 38123, Trento – Italy*

[⊥]*School of Engineering and Materials Science, Queen Mary University of London, Mile End Road, E1 4NS London - United Kingdom*

[∞] *Ket Lab, Edoardo Amaldi Foudation, Italian Space Agency, Via del Politecnico snc, 00133 Rome, Italy*

Keywords: Graphene, protective layer, PDMS, water, air bubble, AFM, captive contact angle, graphite, wettability, XPS, Raman.

Corresponding author: Ruben Bartali, bartali@fbk.eu, via Sommarive 18 38123, Trento (Italy)

1) Captive Contact Angle and Sessile Contact Angle

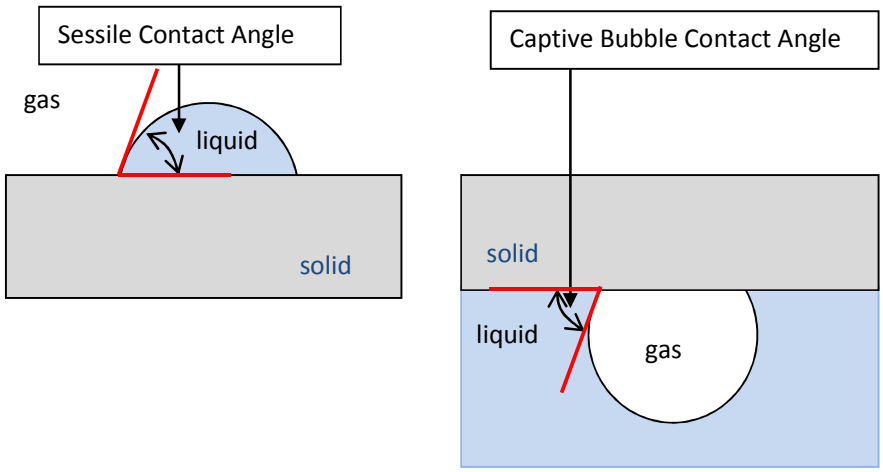

S1. Drop and Bubble in contact with a surface: a) sessile contact angle b) captive contact angle.

2) Roughness evolution in water

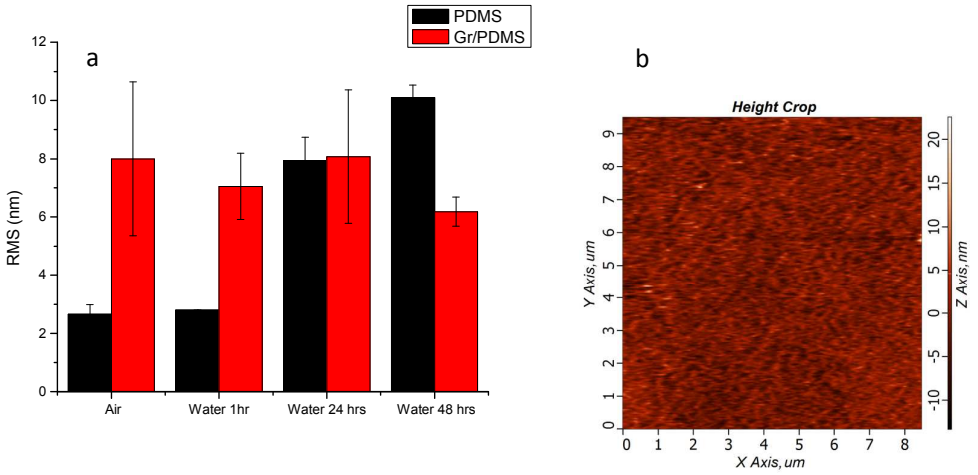

S2. Histogram showing roughness (rms) of PDMS and Gr/PDMS in air and water. The roughness of PDMS is increasing after immersion in water up to 48 hours while graphene covered PDMS are unaltered in roughness. The standard deviation is calculated from data of different regions of the sample (a). Morphology of PDMS in water after 1 hour of immersion (b).

3) Condensed drop inside the bubble

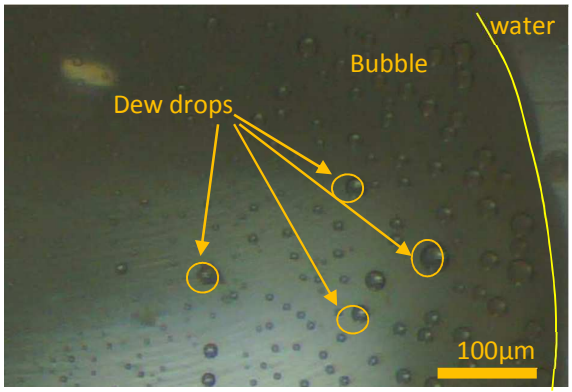

S3. Water vapor condensed inside the bubble region during the measurement by captive angle set-up. The microdrops due to condesation of water vapor have been detected, thanks to the transparency of PDMS and by micro camera on the top side of the captive cell.